On Modeling, Identification, and Control of a Heavy-Duty Electrohydraulic Harvester Manipulator

Evangelos Papadopoulos, *Senior Member, IEEE*, Bin Mu, and Réal Frenette

***Abstract*—This paper focuses on modeling, parameter estimation, and control for a heavy-duty electrohydraulic manipulator of a harvester machine. The linear-graph method is implemented in deriving mathematical models for the swing, boom and stick subsystems. Actuation dynamics are subsequently integrated with manipulator dynamics to result in a complete machine model. Identification procedures employed in estimating physical parameters are discussed in detail and key parameter results supplied. Model validation studies show good agreement between model predictions and experiments. A Cartesian controller for the motion of the manipulator end-point is described and response results are presented. It is shown that the obtained response is very good for the purposes of this harvester machine, resulting in very small relative tracking errors.**

***Index Terms*—Cartesian control, heavy-duty hydraulic manipulators, hydraulic servo control, parameter identification.**

I. Introduction

FOR MANY nations, forestry is the most important industry in terms of people employed and contribution to the economy, [1]. Increased global competition and strict environmental laws require that forestry resources are harvested more efficiently and more carefully than previously. This requires sophisticated forestry equipment with better and easier-to-use controls, increased efficiency, and self-diagnostics. Such equipment will allow operators to concentrate more on planning tree-harvesting operations, [2].

Sophistication in the form of computerized control and diagnostics should not increase costs significantly, while the system should remain reliable in harsh environments. These requirements dictate the use of industrial grade hydraulic actuation systems and computers; i.e., high-end fast workstations and expensive servo-systems are not appropriate. An important challenge is how to achieve superior results available in high performance robotic systems but with existing industrial grade technology. In such cases, improving the performance can be achieved in part by modeling and model-based control. This is the main focus of this paper.

Manuscript received January 20, 2003; revised March 13, 2003. This work was supported by the by the Ministère de l'Industrie, du Commerce, de la Science et de la Technologie (MICST), of Quebec, Canada, under the program SYNERGIE. Recommended by Guest Editors C. Mavroidis and N. Sarkar.

E. Papadopoulos is with the Department of Mechanical Engineering, National Technical University of Athens, 15780 Athens, Greece, (e-mail: egpapado@central.ntua.gr).

B. Mu is with ADEPT, Livermore, CA 94551 USA (e-mail: brian.mu@adept.com).

R. Frenette is with Autolog, Blainville, QC J7C 5S4, Canada (e-mail: realf@autolog.com).

Digital Object Identifier 10.1109/TMECH.2003.812820

Mathematical models are used toward understanding the dynamic characteristics of electrohydraulic actuation systems for designing and implementing control algorithms. The majority of previous work has focused on modeling of individual servovalves, transmission lines and actuators. Mclain *et al.* developed dynamic models for a complete electrohydraulic actuation system, [3]. The models included a single-stage, four-way, suspension-type valve, not used in industry. The high cost of hydraulics, sensors and data-acquisition systems, and the lack of experience in hydraulics, limit research on heavy-duty hydraulics. Due to these reasons, control design and coordination of articulated manipulators are not easy to achieve [4]. Nevertheless, various identification methods for transmission lines [5], [6], actuators [7], and servovalves [8], [9], have been proposed and implemented, and specific servo actuation systems have been investigated [3], [10], [11]. Control studies in hydraulics have typically concentrated on single-cylinder, servo-control applications in a simulation or a laboratory environment. The control approaches employed include adaptive, robust, or time-delayed control laws, see for example [12]–[14].

Little research has been reported in the area of heavy-duty industrial or field manipulators. Most of the available work is control related. A resolved-mode controller has been applied on a heavy-duty excavator. The authors dealt successfully with the particular hydraulics found in excavator machines [15]. A feedforward controller with desired trajectory based adaptation was employed experimentally in the control of a heavy-duty industrial manipulator. Results were promising but indicated that the response improvement did not justify the additional sensors and controller complexity, [16]. A time-delayed control approach has been applied in excavator end-point motions with good performance, [17].

In this paper, the dynamic behavior of the electrohydraulic actuation system of a heavy-duty harvester manipulator is studied first. Models describing such behavior are needed in the development of training simulators, in control system design, and in the detection of failures. The linear graph method is implemented in deriving mathematical models of three actuation subsystems used on the vehicle, namely, the swing, boom, and stick subsystems. The actuation dynamics are integrated with rigid body dynamics to result in a complete manipulator model. Identification procedures employed in estimating physical parameters are discussed in detail. Model-validation studies are carried out that show good agreement between the model and experiments in both open and closed loop experiments. The derived models can be used in designing advanced controllers, in system fault detection and prediction, and in graphical training simulators. Finally, a manipulator Cartesian

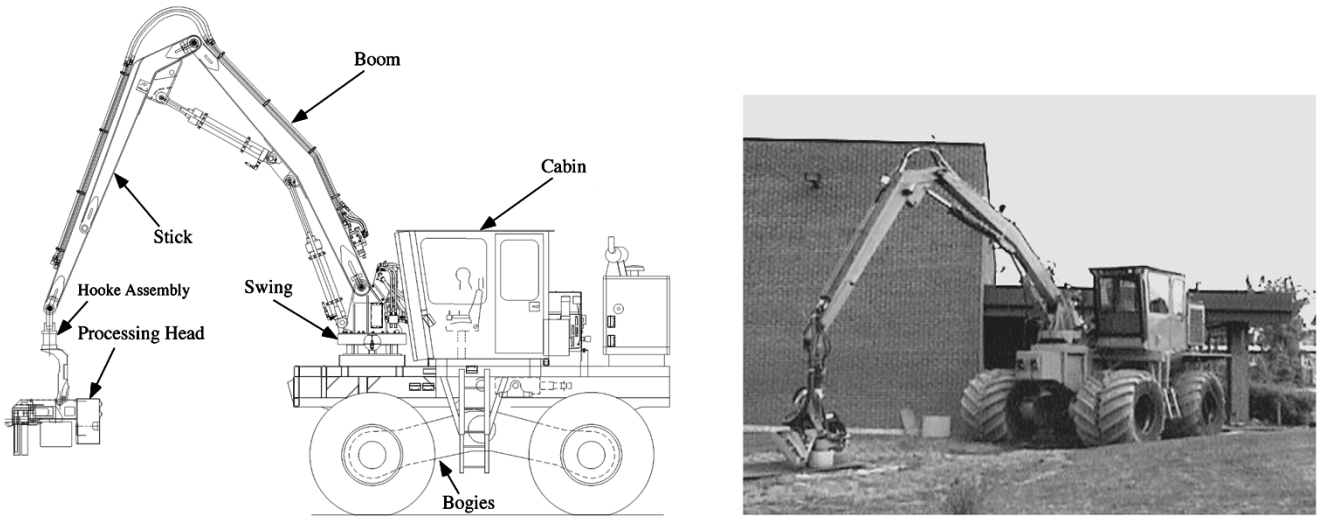

Fig. 1. FERIC harvester machine and its manipulator.

controller is developed and response results are presented. It is shown that the obtained response is very good for the purposes of this harvester machine, resulting in very small relative tracking errors.

II. Harvester Manipulator

The work described here was part of a Canadian initiative in forestry robotics, called "ATREF" (Application des Technologies Robotiques aux Équipements Forestiers), [2]. The 20-ton harvester machine used was provided by the Forest Engineering Research Institute of Canada (FERIC), and was equipped with an articulated manipulator that includes a hydraulic motor-actuated swing joint, and cylinder-actuated boom and stick joints, see Fig. 1. A Hooke-type assembly at the end point permits free swinging of the processing head in two degrees of freedom (dof), see Fig. 1.

The manipulator's workspace has a diameter of 15 m and a height of 10 m, while the payload is 700 kg. Two constant-pressure pumps are driven by a diesel engine, rated 152 hp at 2500 r/m and supply a pressure of 3000 psi to the hydraulic actuators.

Velocity commands, issued by an on-board operator via an appropriate joystick, are processed by an embedded industrial computer system and, as a result, voltages are sent to proportional valves.

III. System Dynamics

The dynamic characteristics of the hydraulic systems are intricate due to the large number of components involved and their nonlinear behavior. Access to a dynamics model of such a system allows for understanding and designing closed-loop controllers, for designing training simulators, and for detecting system failures by running models in parallel to operations. To achieve the desired level of accuracy in modeling and estimating the corresponding parameters, the system was broken into its components. Each of these is modeled individually, and the overall dynamic model is assembled from the individual models. The components modeled include pumps, proportional valves, hoses, cylinders, and the swing motor. Linear graphs were chosen as the modeling methodology, [18].

a) Pumps: Two pressure-compensated, piston pumps provide constant pressure to the test vehicle, and are modeled as ideal pressure sources, see Figs. 2 and 3.

b) Valves: Three two-stage, four-way proportional spool valves are used to actuate the swing, boom and stick subsystems. Only the resistive effect of the valves is considered in the dynamic models, due to the fact that their natural frequency is much higher than that of the hydraulics and manipulator. It is also assumed that the fluid and the geometry of the valves are ideal (e.g., sharp edges), [19]. The valve resistance, is given by the orifice equation

$$\Delta P = C_R \cdot Q \cdot |Q| \tag{1}$$

where ΔP is the pressure difference across the valve, Q is the flow through the valve, and C_R is a coefficient which is function of fluid density ρ, the orifice area A, and the discharge coefficient C_d

$$C_R = 0.5 \cdot \rho \cdot C_d^{-2} \cdot A^{-2}. \tag{2}$$

Input voltage commands modulate the orifice areas, which affect the magnitude of C_R. For most sliding-type valves at small openings, C_d is fairly constant when the Reynolds number is greater than 260. If the orifice edges are sharp, as assumed previously, then the discharge coefficient is $C_d = 0.60$ to 0.65, [20].

c) Hoses: A lumped-parameter modeling methodology is applied to derive transmission line models. Its validity depends on whether the observed frequency of oscillation in the actuation system, is significantly lower than the frequency corresponding to wave propagation, [21]. This criterion can be expressed as

$$l_h < 0.5 \cdot C_0 \cdot f^{-1} = l_{\rm cr}, \quad \text{with} \quad C_0 = \beta^{1/2} \cdot \rho^{-1/2} \tag{3}$$

where f is the line-oscillation frequency observed (about 3 Hz), l is the hose length, C_o is the velocity of sound in the oil, and β is its bulk modulus. For the oil used, $\beta = 1.6 \times 10^9$ N/m^2,

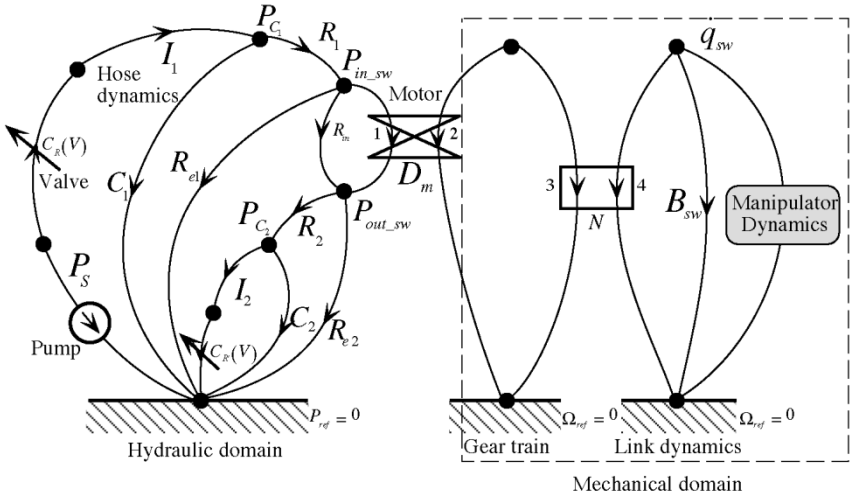

Fig. 2. Swing subsystem model.

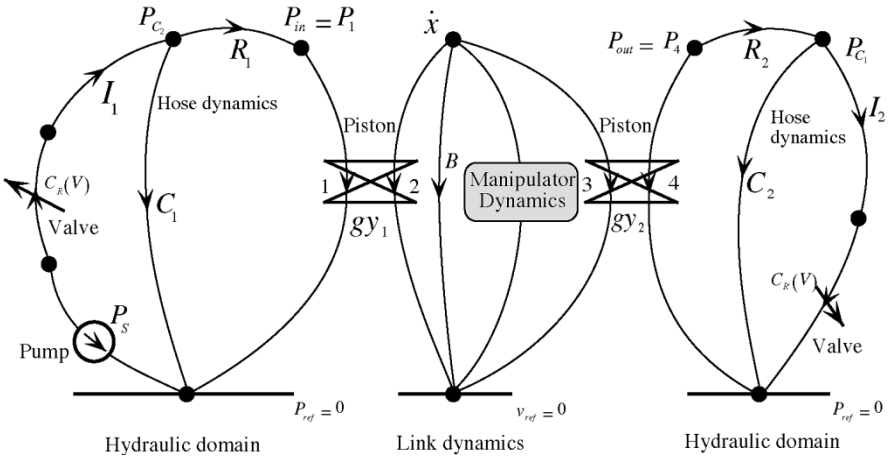

Fig. 3. Boom and stick linear graphs.

$\rho = 970$ kg/m^3, resulting in $l_{\rm cr}$ equal to 214 m. Therefore, to develop a model that describes well the behavior of the hoses, one lump is sufficient, even for the longest machine hose, for which $l_h = 4$ m.

The following modeling assumptions were made.

1) Turbulent flow is assumed (nonlinear pressure-flow relationship) for the boom and stick. In contrast, laminar flow is assumed for the swing model due to the fact that the swing hoses are very short, and turbulent flow can not develop completely.
2) Fluid compressibility and line compliance effects are linear. They hold for relatively small pressure fluctuations from the steady state pressure and for small expansion in the hoses.
3) In defining fluid inertance, the momentum of the fluid on the inlet and outlet sides of a control volume is assumed to be the same.

There are many alternatives for arranging inertance, capacitance, and resistance elements for a hose model. Here, a common "T" type is used, in which the resistance and inertance are in series, and the capacitance is connected at their common node, see Figs. 2 and 3. This was dictated by the need for a smaller model and by sensor availability and feasible installation locations.

d) Hydraulic Cylinders: Two single-ended (asymmetrical) cylinders are used to actuate the boom and stick. It is assumed that cylinder chambers are rigid, that dominant friction effects in the piston seals are viscous, (the oil lubricates the seals and greatly reduces the effect of coulomb friction), and that there is no significant leakage past the piston; leakage is further prevented by the piston's single-ended configuration. Since hydraulic cylinders convert fluid to mechanical power, this transduction is modeled in linear graphs as a gyrator. Due to the single-ended configuration, the common two-port element gyrator cannot be applied directly. Instead, two two-port gyrators are used, see Fig. 3.

e) Hydraulic Motor: fixed-displacement piston motor is used to drive the swing. Contrary to cylinders, hydraulic motors can be modeled as single two-port gyrators, see Fig. 2. The following assumptions are made.

1) Viscous friction of the motor is lumped into the damping of the gear train connected to its output shaft.
2) Internal and external motor leakage is present, and slip flow is laminar.

Although in general, the volumetric efficiency of hydraulic motors is quite high, at low speeds the slip-flow effect becomes more prominent. Very often, the swing motor is working within this speed range.

f) Other Components: Filters and check valves are present which behave as fluid resistances. However, specifications show that their resistance is much smaller than that of the valves, and hoses. Therefore, their effect is neglected.

Based on the above, the linear graph of the swing subsystem was constructed as shown in Fig. 2, where P_s is the pump pressure; C_R, $C_{R'}$ are the valve-orifice resistances modulated by the input (command) voltage; I_1, I_2, C_1, C_2, and R_1, R_2, are the supply and return-line inertance, capacitance, and resistance; R_{in}, R_{e1}, R_{e2} are the internal and external leakage of the motor whose volumetric displacement is D_m; N is the gear train gear ratio; B_{sw} is the gear train viscous damping; and $\dot{q}_{\text{sw}}$ the swing angular velocity.

Similarly, the boom and stick models are constructed as shown in Fig. 3. Additional parameters include the rod and head areas of the piston $gy_1 = A_1$, and $gy_2 = A_2$, the cylinder viscous damping B, and $\dot{x}$ the piston velocity.

The dynamic models of the manipulator were derived separately, and have the form [22]

$$\mathbf{M}(\mathbf{q}) \cdot \ddot{\mathbf{q}} + \mathbf{V}(\mathbf{q}, \dot{\mathbf{q}}) + \mathbf{G}(\mathbf{q}) = \boldsymbol{\tau} \tag{4}$$

where $\mathbf{M}(\mathbf{q})$ is a mass matrix, $\mathbf{V}(\mathbf{q}, \dot{\mathbf{q}})$ includes Coriolis and centrifugal terms, $\mathbf{G}(\mathbf{q})$ includes gravity terms, and $\boldsymbol{\tau}$ is the joint input torque provided by the actuators. To integrate this model to the hydraulic actuator models, one needs to provide expressions transforming pressure differences to forces or torques, and angular velocities to flows.

For the two cylinders, the actuator to joint space differential kinematics are given by

$$\dot{\mathbf{x}} = \mathbf{J} \cdot \dot{\mathbf{q}}, \qquad \boldsymbol{\tau}_{\text{cyl}} = \mathbf{J}^{\mathbf{T}} \cdot \mathbf{F} \tag{5}$$

where $\mathbf{x}$ is the vector of piston (actuator) displacements, $\mathbf{q}$ is the vector of manipulator joint angles, $\mathbf{F}$ includes the forces generated by the actuators, and $\boldsymbol{\tau}_{\text{cyl}}$ are the corresponding torques. Since each link is independently actuated, the Jacobian $\mathbf{J}$ is a diagonal matrix. For single-ended cylinders, output forces are related to pressures and flows to linear velocities by the following equations:

$$\begin{bmatrix} F_{\text{bm}} \\ F_{\text{sk}} \end{bmatrix} = \begin{bmatrix} A_{\text{in\_bm}} & -A_{\text{out\_bm}} & 0 & 0 \\ 0 & 0 & A_{\text{in\_sk}} & -A_{\text{out\_sk}} \end{bmatrix} \cdot \begin{bmatrix} P_{\text{in\_bm}} \\ P_{\text{out\_bm}} \\ P_{\text{in\_sk}} \\ P_{\text{out\_sk}} \end{bmatrix} \tag{6a}$$

$$\begin{bmatrix} Q_{\text{in\_bm}} \\ Q_{\text{in\_sk}} \\ Q_{\text{out\_bm}} \\ Q_{\text{out\_sk}} \end{bmatrix} = - \begin{bmatrix} A_{\text{in\_bm}} & 0 \\ 0 & A_{\text{in\_sk}} \\ A_{\text{out\_bm}} & 0 \\ 0 & A_{\text{out\_sk}} \end{bmatrix} \begin{bmatrix} \dot{x}_{\text{bm}} \\ \dot{x}_{\text{sk}} \end{bmatrix} \tag{6b}$$

where $A_{\text{in\_bm}}$, $A_{\text{out\_bm}}$, $A_{\text{in\_sk}}$, $A_{\text{out\_sk}}$ are driving and returning areas of the boom and stick pistons; F_{bm}, F_{sk} are the forces generated by boom and stick cylinders. Similarly, $P_{\text{in\_bm}}$, $P_{\text{out\_bm}}$, $P_{\text{in\_sk}}$, $P_{\text{out\_sk}}$ are pressures at inlet and outlet of the boom and stick cylinders, and $Q_{\text{in\_bm}}, Q_{\text{out\_bm}}, Q_{\text{in\_sk}}, Q_{\text{out\_sk}}$ are flow rates. The negative sign in the second equation is due to linear graph conventions. The full transduction equations are

$$\begin{aligned} \begin{bmatrix} \tau_{\text{bm}} \\ \tau_{\text{sk}} \end{bmatrix} &= \boldsymbol{\tau}_{\text{cyl}} \\ &= \mathbf{J}^T(\mathbf{q}) \cdot \mathbf{F} = \mathbf{J}^T(\mathbf{q}) \cdot \begin{bmatrix} F_{\text{bm}} \\ F_{\text{sk}} \end{bmatrix} \\ &= \mathbf{J}^T \begin{bmatrix} A_{\text{in\_bm}} & -A_{\text{out\_bm}} & 0 & 0 \\ 0 & 0 & A_{\text{in\_sk}} & -A_{\text{out\_sk}} \end{bmatrix} \\ &\quad \cdot \begin{bmatrix} P_{\text{in\_bm}} \\ P_{\text{out\_bm}} \\ P_{\text{in\_sk}} \\ P_{\text{out\_sk}} \end{bmatrix} \end{aligned} \tag{7a}$$

$$\begin{aligned} \begin{pmatrix} \dot{q}_{\text{bm}} \\ \dot{q}_{\text{sk}} \end{pmatrix} &= \mathbf{J}^{-1} \begin{bmatrix} \dot{x}_{\text{bm}} \\ \dot{x}_{\text{sk}} \end{bmatrix} \\ &= -\mathbf{J}^{-1} \begin{bmatrix} 1/A_{\text{in\_bm}} & 0 \\ 0 & 1/A_{\text{in\_sk}} \end{bmatrix} \begin{bmatrix} Q_{\text{in\_bm}} \\ Q_{\text{in\_sk}} \end{bmatrix} \\ &= -\mathbf{J}^{-1} \begin{bmatrix} 1/A_{\text{out\_bm}} & 0 \\ 0 & 1/A_{\text{out\_sk}} \end{bmatrix} \begin{bmatrix} Q_{\text{out\_bm}} \\ Q_{\text{out\_sk}} \end{bmatrix}. \end{aligned} \tag{7b}$$

The transduction equation for the swing motor is simpler

$$\begin{bmatrix} \dot{q}_{\text{sw}} \\ \tau_{\text{sw}} \end{bmatrix} = \begin{bmatrix} 0 & 1/(D_m N) \\ -D_m N & 0 \end{bmatrix} \begin{bmatrix} P_{\text{in\_sw}} - P_{\text{out\_sw}} \\ Q_{\text{sw}} \end{bmatrix}. \tag{8}$$

The relationship between manipulator dynamics, described by $\boldsymbol{\tau}$ and $\dot{\mathbf{q}}$ and electrohydraulic actuator dynamics, described by pressures and flows are set up next. The system equations for the 3-dof manipulator consist of eighteen first-order nonlinear differential equations given below

$$\begin{aligned} \dot{\mathbf{q}}_{\mathbf{1}} &= \mathbf{q}_{\mathbf{2}} \\ \dot{\mathbf{q}}_{\mathbf{2}} &= \mathbf{M}(\mathbf{q}_{\mathbf{1}})^{-\mathbf{1}} \{ -\mathbf{V}(\mathbf{q}_{\mathbf{1}}, \mathbf{q}_{\mathbf{2}}) - \mathbf{G}(\mathbf{q}_{\mathbf{1}}) + \boldsymbol{\tau} \} \\ \dot{P}_{c_1\_\text{sw}} &= C_{1\_\text{sw}}^{-1} (Q_{i_1\_\text{sw}} - (P_{C_1\_\text{sw}} - P_{R_{\text{in}}} \\ &\qquad \cdot(\dot{q}_{\text{sw}}) - P_{R_2} - P_{C_2\_\text{sw}}) / R_1) \\ \dot{P}_{c_2\_\text{sw}} &= \{ (P_{C_1\_\text{sw}} - P_{R_{\text{in}}}(\dot{q}_{\text{sw}}) - P_{R_2} - P_{C_2\_\text{sw}}) / R_1 \\ &\qquad - (P_{R_{\text{in}}}(\dot{q}_{\text{sw}}) + P_{R_2} + P_{C_2\_\text{sw}}) / R_{e_1} \\ &\qquad - (P_{C_2\_\text{sw}} + P_{R_2}) / R_{e_2} - Q_{i_2\_\text{sw}} \} / C_{2\_\text{sw}} \\ \dot{Q}_{i_1\_\text{sw}} &= \left(P_s - C_R \cdot Q_{i_1\_\text{sw}}^2 \cdot \text{sign}(Q_{i_1\_\text{sw}}) - P_{C_1\_\text{sw}} \right) / I_{1\_\text{sw}} \\ \dot{Q}_{i_2\_\text{sw}} &= \left(P_{C_2\_\text{sw}} - C_{R'} \cdot Q_{i_2\_\text{sw}}^2 \cdot \text{sign}(Q_{i_2\_\text{sw}}) \right) / I_{2\_\text{sw}} \\ \dot{P}_{c_1\_\text{bm}} &= (Q_{i_1\_\text{bm}} - gy_1 \cdot \dot{x}_{\text{bm}}) / C_{1\_\text{bm}} \\ \dot{P}_{c_2\_\text{bm}} &= (gy_2 \cdot \dot{x}_{\text{bm}} - Q_{i_2\_\text{bm}}) / C_{2\_\text{bm}} \\ \dot{Q}_{i_1\_\text{bm}} &= \left(P_s - C_R \cdot Q_{i_1\_\text{bm}}^2 \right. \\ &\qquad \left. \cdot \text{sign}(Q_{i_1\_\text{bm}}) - P_{c_1\_\text{bm}} \right) / I_{1\_\text{bm}} \\ \dot{Q}_{i_2\_\text{bm}} &= \left(P_{c_2\_\text{bm}} - C_{R'} \cdot Q_{i_2\_\text{bm}}^2 \cdot \text{sign}(Q_{i_2\_\text{bm}}) \right) / I_{2\_\text{bm}} \\ \dot{P}_{c_1\_\text{sk}} &= (Q_{i_1\_\text{sk}} - gy_1 \cdot \dot{x}_{\text{sk}}) / C_{1\_\text{sk}} \\ \dot{P}_{c_2\_\text{sk}} &= (gy_2 \cdot \dot{x}_{\text{sk}} - Q_{i_2\_\text{sk}}) / C_{2\_\text{sk}} \\ \dot{Q}_{i_1\_\text{sk}} &= \left(P_s - C_R \cdot Q_{i_1\_\text{sk}}^2 \cdot \text{sign}(Q_{i_1\_\text{sk}}) - P_{c_1\_\text{sk}} \right) / I_{1\_\text{sk}} \\ \dot{Q}_{i_2\_\text{sk}} &= \left(P_{c_2\_\text{sk}} - C_{R'} \cdot Q_{i_2\_\text{sk}}^2 \cdot \text{sign}(Q_{i_2\_\text{sk}}) \right) / I_{2\_\text{sk}} \end{aligned} \tag{9a}$$

TABLE I
LINK INERTIAL PROPERTIES

	M [kg]	I_{xx} [kgm^2]	I_{yy} [kgm^2]	I_{zz} [kgm^2]
Swing	907	52	53	56
Boom	635	17	756	833
Stick	545	16	535	867

where

$$\mathbf{q_1} = [\, q_{\rm sw} \quad q_{\rm bm} \quad q_{\rm sk} \,]^T, \qquad \boldsymbol{\tau} = [\, \tau_{\rm sw} \quad \tau_{\rm bm} \quad \tau_{\rm sk} \,]^T. \tag{9b}$$

IV. EXPERIMENTAL IDENTIFICATION

The enormous size, weight, and power of the experimental system, as well as the industrial environment in which this was made available for experimentation, made identification experiments quite challenging. Two sets of parameters were estimated or identified: a) Rigid body parameters; and b) Actuation system parameters.

A. Rigid Body Parameters

a) Component Masses: Link masses are not difficult to find provided that the links can be disassembled from the machine and that huge scales are available. Fortunately, the machine manipulator was partly disassembled during modification works and its links were weighed. Center of mass locations were found using suspension experiments. The results of these measurements are shown in Table I.

b) Component Moments of Inertia: Moments of inertia can be found using a pendulum experiment, during which, a rigid body is suspended from a point, is angularly displaced, and then is set free to swing. Care must be taken so that swinging occurs on a single plane. The period of the resulting oscillation is recorded, and is subsequently used to calculate the moment of inertia around the axis of rotation according to

$$I^0_{zz} = 1/4 \cdot mglT^2\pi^{-2} \tag{10}$$

where I^0_{zz} is the moment of inertia of the body with respect to the axis of swinging (a z axis), m is its mass, T is the period of oscillation, and l is the length from the point of suspension to body center of mass. The moments of inertia with respect to body center of mass are then computed using the parallel axis theorem. As shown by (10), the inertia is proportional to the square of the time period, and this may result in substantial estimation errors. Moreover, swinging a huge body with respect to a single axis is a difficult task. For these reasons, pendulum experiments were used in parallel to solid modeling techniques.

Solid modeling techniques can be used to obtain all mass properties and center-of-mass positions, assuming that the material and the geometry of a body or link are precisely known. However, this is not always the case. To match solid modeling estimates to measurements, static suspension, weighing, and pendulum experiments were used to refine solid models to the point that both the estimated and measured total mass and moment of inertia were in agreement. The solid models generated for the swing and the boom are shown in Fig. 4. Following the techniques described above, the inertia parameters of the links were obtained and are given in Table I.

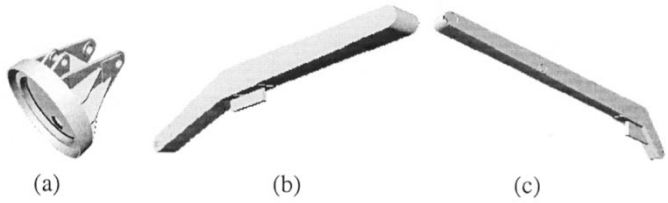

Fig. 4. Solid models for the (a) swing, (b) boom, and (c) stick.

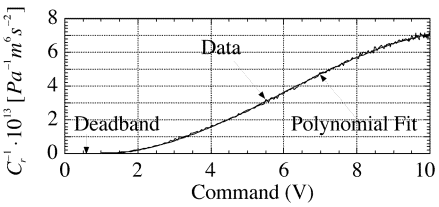

Fig. 5. Valve $C_R^{-1}(V)$ experimental data and fitted curve.

B. Actuation System Parameters

The majority of the actuation system parameters were identified individually in order to minimize estimation errors. The damping associated with the joints was estimated using least-square techniques after all other parameters were identified. The data-acquisition system used included a STD32-bus Ziatech-8902, 486 DX-2 computer installed at the back of the cabin on the vehicle. The data were collected under the QNX real-time operating system at a rate of 200 Hz, and sent to a remote QNX-based 486 DX-2 computer via an Ethernet connection.

a) Valves: Since the three proportional valves used for the swing, boom, and stick are identical, one of them was tested experimentally and its C_R calculated. By varying the magnitude of voltage commands, several sets of pressures $P_{\rm in}$, $P_{\rm out}$ and flow rates Q were collected. Using (1) and a curve-fitting algorithm, a third-order polynomial representation of $C_R^{-1}(V)$ was found, see Fig. 5. Fitting C_R, instead of its inverse, is more difficult due to the large C_R values during valve closure, and usually it requires more than one polynomial to achieve acceptable curve-fitting. The region between 0 and 1.2 V corresponds to valve deadband.

b) Hose Resistance: For incompressible, fully developed turbulent flow in hoses, the pressure drop is related to flow according to (1). To estimate hose C_R, a SAE 100R12 hose of 4 meters in length and 3/4″ in diameter was connected to valve ports A and B. The valve orifice was changed so as to obtain different steady flows. The flow was measured by an FTI Flow Technology turbine sensor, placed at the middle of the hose, while the two pressures were measured by Webster LPT sensors placed at hose ends. Fig. 6 shows the results, where the solid line represents experimental measurements and the dotted line is the polynomial curve fitting result, i.e., $C_R = 3.125E-11$ Pa/(m^3/sec)^2. The flat region at the beginning of the solid line is due to flow sensor limitations.

The SAE 100R12 very-high-pressure hydraulic hose is the only type of hose used on the vehicle. For hoses with different

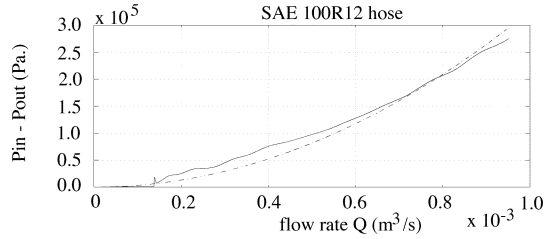

Fig. 6. Hose resistance measurement.

diameters and lengths, their resistance can be calculated using the following exact formula, [20]

$$\Delta P = \alpha \mu^{0.25} \rho^{0.75} L D^{-4.75} Q^{1.75} \Rightarrow \Delta P Q^{1.75} \propto L D^{-4.75} \tag{11}$$

where α is a constant depending on the units, μ is the absolute oil viscosity, ρ is the oil density, L is the pipe length, and D is the inside diameter of the pipe. To obtain a new C_R, $Q^{1.75}$ is approximated by $Q \cdot |Q|$.

c) Inertance and Capacitance: The line inertance and capacitance are estimated from pressure and flow rate readings based on element equation definitions, [18]. To this end, a simple T-model was assumed, see Figs. 2 and 3. At the ends of the hose, a flow and a pressure sensor were added. Using the valve, line transients were induced, and the inlet and outlet pressures, P_1, and P_2, and the inlet and outlet flow, Q_1, and Q_2, were recorded. Using element equations, the capacitance and inertance were approximated by

$$C = (Q_1 - Q_2)(dP_3/dt)^{-1} \tag{12}$$

$$I = (P_1 - P_3)(dQ_1/dt)^{-1}. \tag{13}$$

Pressure P_3 corresponds to pressure P_{Ci} in Figs. 2 and 3 and was estimated as

$$P_3 = R \cdot Q_2 \cdot |Q_2| + P_2. \tag{14}$$

For a machine hose with length of 4 m and diameter of 3/4″, four groups of data, corresponding to different excitations, were collected. The mean values for the inertance and capacitance were calculated from each group. Averaging these yielded, $C = 1.59 \times 10^{-12}$ m^5/N, and $I = 3.01 \times 10^7$ kg/m^4.

d) Motor Leakage: Two types of leakage flows exist in hydraulic motors: the internal or cross-port leakage between higher and lower pressure chambers, and the external leakage from each motor chamber passing through motor pistons to the case drain. Because all clearances in a motor are intentionally made small to reduce losses, these leakage flows are laminar and, therefore, proportional to pressure differences.

The internal leakage, R_{in}, is proportional to the pressure difference across the inlet and outlet motor ports, ΔP

$$\Delta P = P_1 - P_2 = R_{\text{in}} \cdot Q_{\text{in}} \tag{15}$$

where Q_{in} is the internal flow. To calculate R_{in}, the manipulator is rotated by 90° from its normal forward position with respect to the swing motor axis. Then, the platform of the harvester is tilted in order to use gravity to rotate the swing motor. With the swing valve completely shut, the manipulator rotates slowly under the effect of gravity, due to the existence of the internal leakage. Measuring the swing angular speed $\dot{\theta}_m$ with the swing resolver yields the internal flow according to

$$Q_{\text{in}} = D_m \cdot \dot{\theta}_m. \tag{16}$$

Measuring ΔP at the motor and using (15) and (16) yields R_{in} as a function of time, see Fig. 7(a). Time averaging such results yields $R_{\text{in}} = 8.0 \times 10^{11}$ N·s/m^5.

The external leakage in each piston chamber is proportional to the chamber pressure and can be written as

$$P_1 = R_{\text{ex}} \cdot Q_{\text{ex1}}, \qquad P_2 = R_{\text{ex}} \cdot Q_{\text{ex2}} \tag{17}$$

where R_{ex} is the external resistance, P_1 is the pressure in forward chamber, P_2 is pressure in return chamber, and Q_{ex1} and Q_{ex2} the corresponding leakages. To estimate R_{ex}, the swing motor was commanded to rotate at steady conditions. Pressures at its ports, as well as leakage from its drain port were measured. Then, the R_{ex} is found as

$$R_{\text{ex}} = (\overline{P}_1 + \overline{P}_2)/Q_{\text{ex}} = (\overline{P}_1 + \overline{P}_2) \cdot \Delta t / V_{\text{ex}} \tag{18}$$

where V_{ex} is the volume of oil collected over a period Δt. The results of seven independent experiments shown in Fig. 7(b) yield $R_{\text{ex}} = 2.1 \times 10^{12}$ N·s/m^5.

e) Friction Parameters: The manipulator is subject to both Coulomb and viscous friction at all manipulator joints, piston seals, and motor gear train. Because it was not possible to measure the force or torque at the verge of motion due to experimental limitations, only viscous friction was estimated after all other parameters were identified, and any accumulative errors were lumped into it.

By assuming all other parameters known, and by driving the system at a constant joint velocity, Equations (4) and (5) can be rewritten into the form of $\dot{q}_{\text{sw}} \cdot B = a$ for the swing, and $\dot{x} \cdot B = a$ for the boom and stick subsystems. Using a number of experimental sets and a least squares approach yielded the damping coefficients given in Fig. 8. The average values were $B_{\text{sw}} = 2.5 \times 10^4$ N·m/(rad·s^{-1}) and $B_{\text{sk}} = B_{\text{bm}} = 1.0 \times 10^5$N/(m·s^{-1}).

V. Model Validation

Open-loop validation. The model given by (9) was implemented in Simulink. To validate it, various input voltage commands were fed to the valves, and simulated responses were compared to experimentally obtained ones. Fig. 9(a) displays the response of key swing subsystem variables, for a triangular input command. The solid line stands for actual measurements and the dotted line is for predicted ones using the derived dynamic models.

The prediction of angular displacements and speeds is very close to the actual ones. The flow-rate prediction is also very good because of its relation to angular rates. The predicted pressure profiles are close to the real ones, although some of the peaks were slightly underestimated. This may be partly due to small discrepancies between the actual and the calculated mass properties, and the fact that a processing head was attached via 2-dof pendulum at the manipulator end-point just before the experiments were conducted. Periodic motions of the

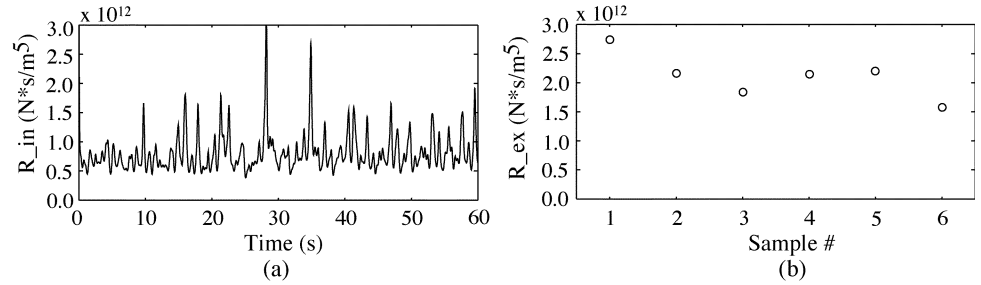

Fig. 7. (a) Internal and (b) external swing motor leakage.

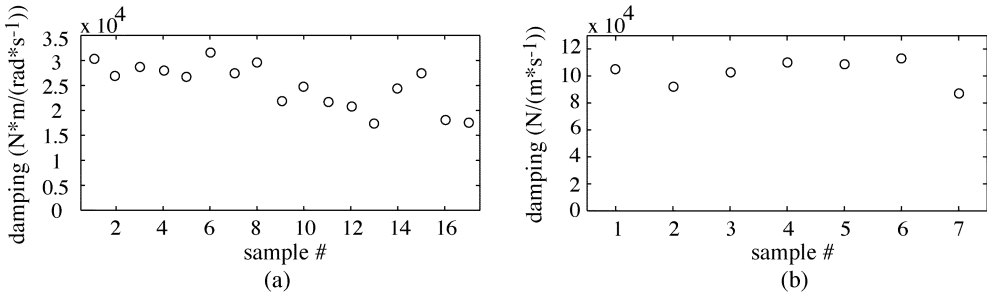

Fig. 8. Viscous friction coefficients for: (a) the swing and (b) the stick.

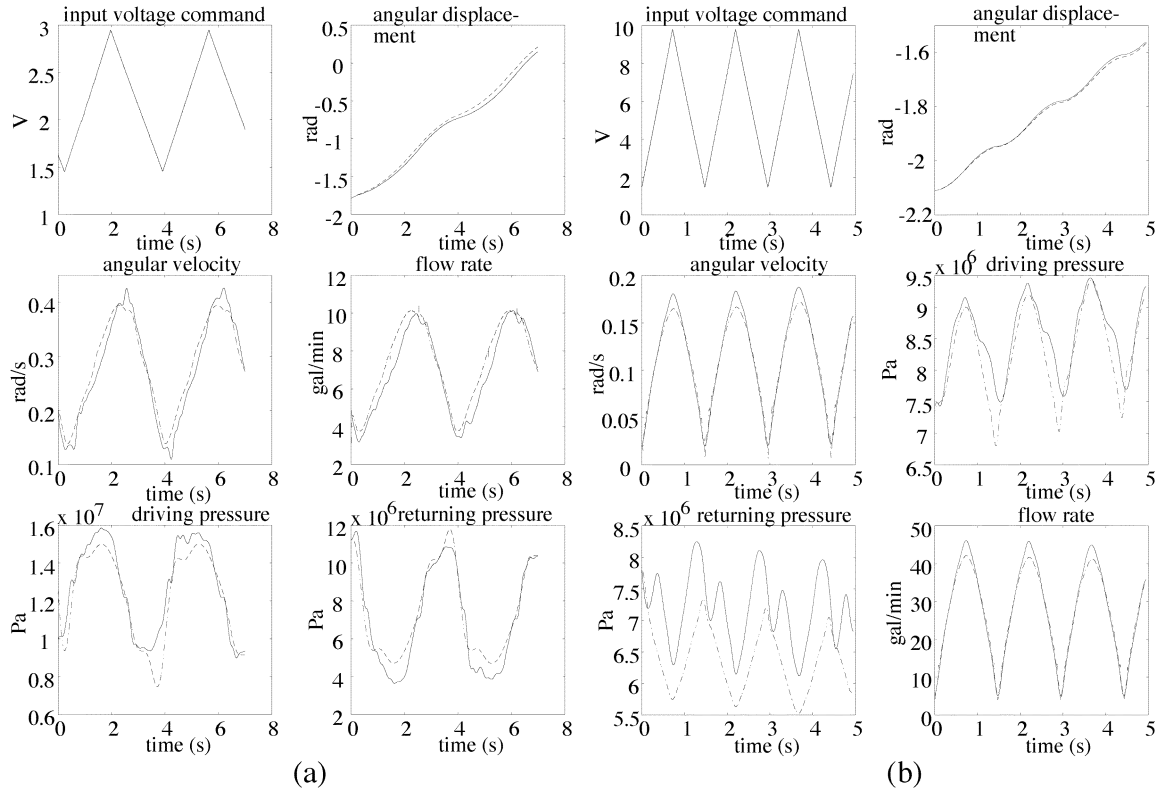

Fig. 9. Model validation studies for: (a) swing and (b) stick.

manipulator caused swinging motions of this head. Although its mass properties were known, and taken into account, the dynamic effects of this motion were neglected due to the lack of pendulum sensors. A more accurate friction model might also contribute in improving the results to some extent. However, the developed models predict well the motions of the manipulator and are considered good enough for the reasons for which they were developed. Results for the other dofs are similar to those presented here. For example, Fig. 9(b) depicts the response of key variables for the stick.

Closed-loop validation. A PID controller was implemented at the joint level, without the feedforward part, see Fig. 10. Resolvers were used for joint angle feedback, while velocities were computed.

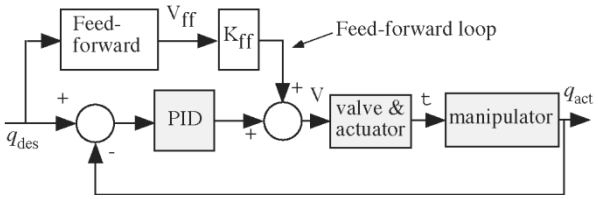

Fig. 10. Joint space PID controller and actuation system.

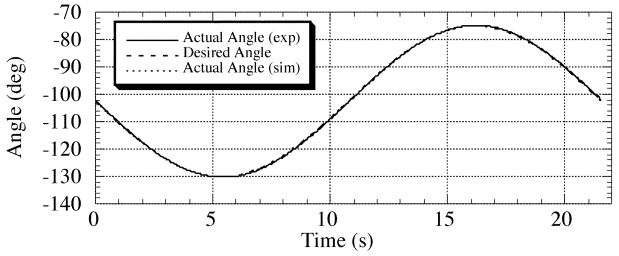

Fig. 11. Desired and actual stick angle response (responses overlapping).

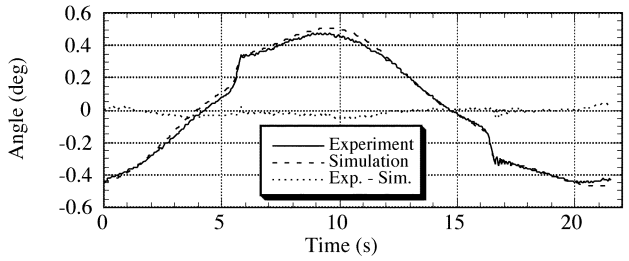

Fig. 12. Comparison of stick experimental and simulated tracking errors.

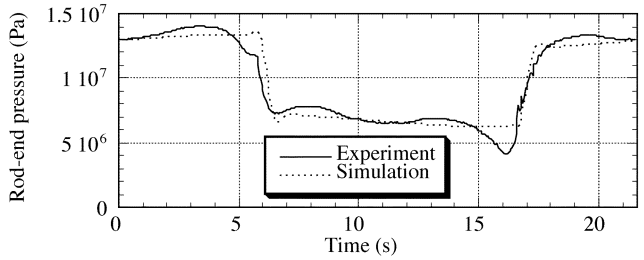

Fig. 13. Comparison of stick rod-end experimental and simulated pressures.

Closed-loop validation for each joint included feeding a sinusoidal angle command to the joint controller. The PID controller used was first introduced in the derived models and appropriate gains were computed for an average configuration. The gains were further tuned by simulations and by experiments on the machine. The same gains were used both in simulation and in experiment. As an example of the response obtained, the stick subsystem response is displayed in Figs. 11–13. The same figures also display the response of the controlled system, simulated in Simulink.

Note that the simulated and actual tracking errors are almost identical. The small oscillations close to 6 and 16s are due to hose dynamics. A simplified model of the actuation system excluding these dynamics predicts accurately the mean response but it is faster, and may therefore be preferred for control or simulation purposes, [23]. Pressure predictions are very good in the mean. Discrepancies are mostly due to load swinging which was not accounted for in the model.

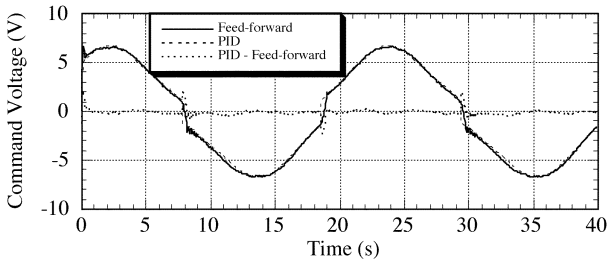

Fig. 14. Feedforward prediction compared to PID voltage command.

VI. Cartesian and Valve Model-Based Control

Originally, the manipulator was controlled at the joint level via a bank of levers. To move the end point in Cartesian space and reach a tree, the operator had to do the inverse kinematics mentally. The new system that was developed allowed for coordinated control of the end-point in Cartesian space or polar coordinate space. To implement this control system, a 3-dof armchair-mounted, heavy-duty joystick, rugged joint resolvers, pressure transducers, and an embedded industrial-grade computer system were installed on the harvester.

The control system running on the computer receives Cartesian speed commands, resolves them into cylinder displacements and sends voltage commands to the joint proportional valves. The joint level controller, depicted in Fig. 10, includes both a feedforward and a feedback part.

Design of the feedforward term is based on the valve characteristic shown in Fig. 5, as follows. Assuming that the tank pressure is zero, the approximate pressure drop at a valve is given by

$$\Delta P_V = P_s - \Delta P_L = P_s - (P_{\text{in}} - P_{\text{out}}). \tag{19}$$

This pressure can be available on-line by measuring P_s, P_{in}, P_{out}. Equation (1) is written as

$$C_R^{-1/2} = Q_V / \sqrt{\Delta P_V} \tag{20}$$

where Q_V is the flow through the valve. A given speed command by the operator allows computation of the desired flow through the valve, $Q_{V,\,des}$. Then, the voltage sent to the valve, V_{ff}, is found using the function shown in Fig. 5 and the following:

$$C_R^{-1/2}(V_{\text{ff}}) = Q_{V,\,des} / \sqrt{\Delta P_V}. \tag{21}$$

As shown in Fig. 10, the feedforward signal is multiplied by a factor K_{ff}. If this feedforward term were all that was needed, then $K_{\text{ff}} = 1$, and no feedback loop would be necessary. However, due to modeling errors and to simplifications made above, K_{ff} is taken less but close to one, and co-exists with the feedback law.

The usefulness of the feedforward controller was first demonstrated off-line. The values recorded during the experiments for closed-loop validation, (trajectory shown in Fig. 11), were fed into a Matlab program that computes the feedforward voltages as explained above. The results are shown in Fig. 14; a difference between the feedforward command estimation and the experimental feedback command is only noticeable when the spool is moving from one side of the valve to the other (i.e.,

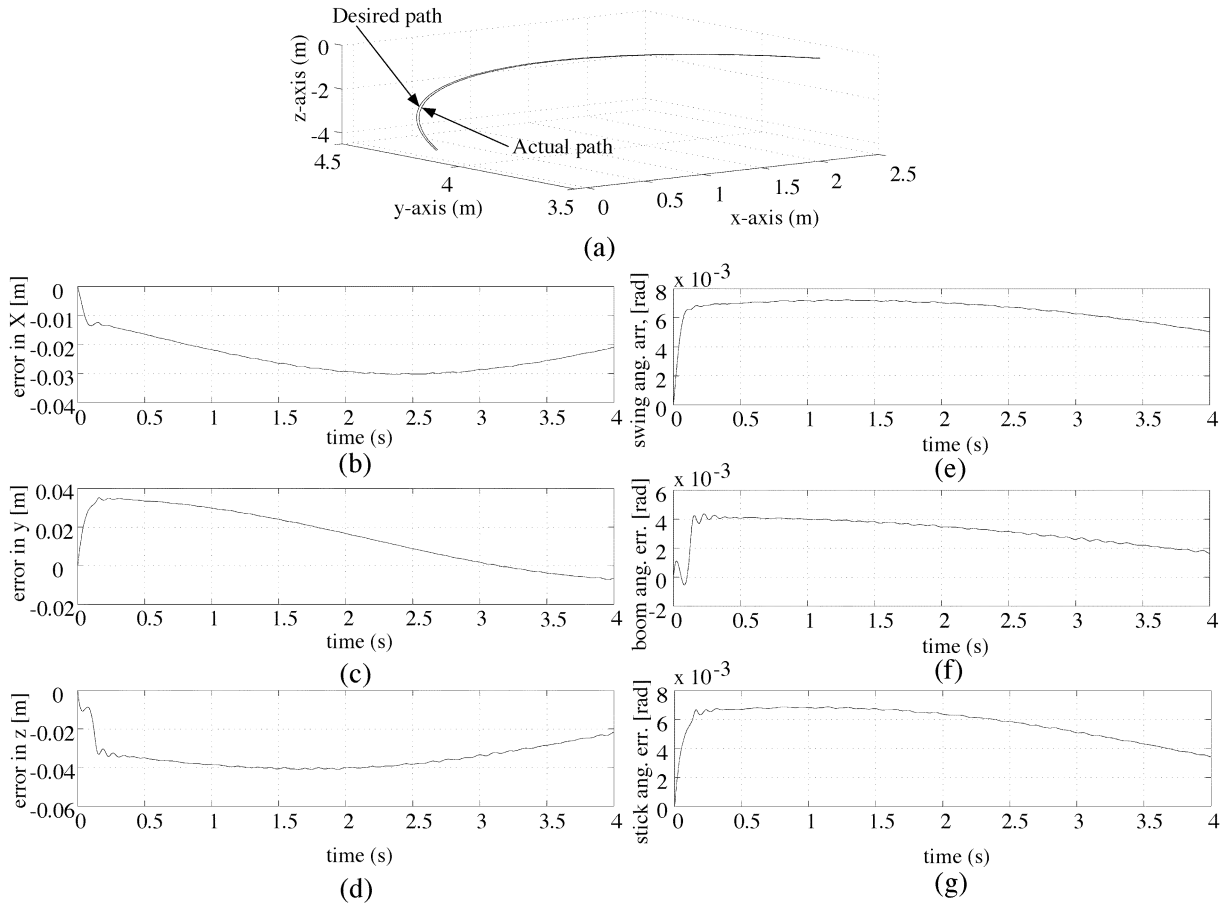

Fig. 15. Cartesian and joint angular errors for the Cartesian motion starting at $(x,\ y,\ z) = (2.0279,\ 3.5139,\ 0.155\,29)$ m and ending at (0.016 382, 4.1488, −4.1062) m. (a) Cartesian path command and response, (b)–(d) Cartesian x, y, z tracking errors, (e)–(g) Joint space tracking errors.

when the polarity of the command changes). Since the valve model provides a good approximation of the voltage needed to produce the desired motion, the feedforward term is proven to be beneficial. More accurate results can be obtained if the valve is modeled as two resistances, one for each port, and an individual C_R for each port is used.

Next, a Cartesian three-dimensional motion of the end-point is evaluated. The endpoint in such machines is commanded by the operator using velocity commands and corrections obtained visually, i.e., the loop with respect to position is closed visually. To yield the commanded path, the velocity commands must be integrated with time.

As an example, the manipulator endpoint is commanded to move in the x–y–z Cartesian space for a distance along the path approximately equal to 5 m, see Fig. 15(a). The resulting path is also presented in the same figure, while the Cartesian and joint space errors are shown in Fig. 15(b)–(d) and (e)–(g). As it can be computed from Fig. 15(b)–(d), the rms tracking error does not exceed 5 cm, and the resulting error is about 1%, i.e., very good for forestry operations.

VII. Conclusion

In this paper, the dynamic behavior of the electrohydraulic system of a heavy-duty harvester manipulator was studied. Linear graphs were employed in deriving models for the swing, boom and stick subsystems. The actuation dynamics were integrated with rigid body dynamics to result in a complete manipulator model. Estimation procedures employed in obtaining values of physical parameters were discussed. Model validation studies showed good agreement between the model and experiments. A Cartesian controller that incorporates a valve-based model was developed and response results were presented. It was shown that the obtained response is very good for the purposes of a harvester machine, resulting in small relative tracking errors. This work indicates that modeling and control can improve the response of heavy-duty hydraulic manipulators and their field effectiveness.

Acknowledgment

The authors wish to thank P. Freedman (CRIM), I. Makkonen (FERIC), R. Germain and J. LeBrun (Denharco), D. Éthier, and R. Lessard (Autolog), and K. Vlachos (NTUA) for their help in various aspects of this work.

References

[1] J. Courteau, "Robotics in Canadian forestry," *Canadian Rev.*, no. winter, pp. 10–13, 1994.

[2] P. Freedman, E. Papadopoulos, D. Poussart, C. Gosselin, and J. Courteau, "ATREF: Application des technologies robotiques aux équipements forestiers," in *Proc. 1995 Canadian Conf. Electrical and Computer Engineering*, Montreal, PQ, Canada, Sept. 5–8, 1995.

[3] T. W. McLain *et al.*, "Development, simulation, and validation of a highly nonlinear hydraulic servosystem model," *Amer. Control Conf.*, pp. 385–391, June 1989.
[4] J. J. Zhou and F. Conrad, "Identification for modeling and adaptive control of hydraulic robot manipulators," in *Proc. 9th IFAC/IFORS Symp. Identification and System Parameter Estimation*, vol. 2, Budapest, Hungary, July 1992, pp. 705–710.
[5] W. C. Yang and W. E. Tobler, "Dissipative modal approximation of fluid transmission lines using linear friction model," *J. Dyn. Syst., Meas., Control*, vol. 113, pp. 152–161, 1991.
[6] P. Krus, K. Weddfelt, and J. Palmberg, "Fast pipeline models for simulation of hydraulic systems," *J. Dyn. Syst., Meas., Control*, vol. 116, pp. 132–136, 1994.
[7] D. L. Wells *et al.*, "An investigation of hydraulic actuator performance trade-offs using a generic model," in *Proc. IEEE Int. Conf. Robotics Automation*, 1990, pp. 2168–2173.
[8] D. J. Martin and C. R. Burrow, "The dynamic characteristics of an electrohydraulic servovalve," *J. Dyn. Syst., Meas., Control*, vol. 98, 1976.
[9] P. N. Nkiforuk *et al.*, "Detailed analysis of a two-stage four-way electrohydraulic flow-control valve," *J. Mech. Eng. Sci.*, vol. 11, no. 2, 1969.
[10] T. Herman *et al.*, "Bond-graph modeling and identification of a high power hydraulic system," in *Proc. 11th IASTED Int. Conf. Modeling, Identification and Control*, Innsbruck, Austria, 1992.
[11] G. Bilodeau and E. Papadopoulos, "Experiments on a high performance hydraulic manipulator joint: Modeling for control," in *Experimental Robotics V*, A. Casals and A. T. de Almeida, Eds. New York: Springer-Verlag, 1998, pp. 532–543.
[12] G. A. Sohl and J. E. Bobrow, "Experiments and simulations on the nonlinear control of a hydraulic servosystem," *Trans. Control Syst. Technol.*, vol. 7, no. 2, pp. 238–247, 1999.
[13] F. Bu and B. Yao, "Integrated direct/indirect adaptive robust motion control of single-rod hydraulic actuators with time-varying unknown inertia," in *Proc. Int. Conf. Advanced Intelligent Mechatronics* , 2001, pp. 624–629.
[14] K. Six, T. A. Lasky, and B. Ravani, "A time-delayed dynamic inversion scheme for mechatronic control of hydraulic system," in *Proc. Int. Conf. Advanced Intelligent Mechatronics*, 2001, pp. 1232–1238.
[15] N. Sepehri, P. D. Lawrence, F. Sassani, and R. Frenette, "Resolved-mode teleoperated control of heavy-duty hydraulic machines," *J. Dyn. Syst., Meas. Control*, vol. 166, no. 2, pp. 232–240, 1994.
[16] M. Honegger and P. Corke, "Model-based control of hydraulically actuated manipulators," in *Proc. IEEE Int. Conf. Robotics Automation*, Seoul, S. Korea, 2001, pp. 2553–2559.
[17] S.-U. Lee and P. H. Chang, "Control of a heavy-duty robotic excavator using time delay control with switching action with integral sliding surface," in *Proc. IEEE Int. Conf. Robotics Automation*, Seoul, S. Korea, 2001, pp. 3995–3960.
[18] D. Rowell and D. Wormley, *System Dynamics*. Englewood Cliffs, NJ: Prentice-Hall, 1997.
[19] J. F. Blackburn *et al.*, *Fluid Power Control*. Cambridge, MA: MIT Press, 1960.
[20] H. E. Merritt, *Hydraulic Control Systems*. New York: Wiley, 1967.
[21] J. Watton, *Fluid Power Systems*. Englewood Cliffs, NJ: Prentice-Hall, 1989.
[22] E. Papadopoulos and S. Sarkar, "The dynamics of an articulated forestry machine and its applications," in *Proc. IEEE Int. Conf. Robotics Automation*, Albuquerque, NM, Apr. 21–27, 1997, pp. 323–328.
[23] E. Papadopoulos and Y. Gonthier, "On the development of a real-time simulator engine for a hydraulic forestry machine," *Int. J. Fluid Power*, vol. 3, no. 1, pp. 55–65, 2002.

Evangelos Papadopoulos (S'83–M'91–SM'97) received the Diploma from the National Technical University of Athens (NTUA), Athens, Greece, in 1981, and the M.S. and Ph.D. degrees from Massachusetts Institute of Technology, Cambridge, in 1983 and 1991, respectively, all in mechanical engineering.

He was an analyst with the Hellenic Navy, Athens, Greece, from 1985 to 1987. In 1991, he joined the Centre for Intelligent Machines (CIM), McGill University, Montreal, QC, Canada, as an Assistant Professor and was tenured in 1997. Currently, he is an Associate Professor in the Mechanical Engineering Department at the NTUA. He teaches courses in the areas of systems, controls, mechatronics, and robotics. His research interests are in the area of robotics, modeling and control of dynamic systems, haptic devices, mechatronics and design. He has published more that 80 articles in journals and conference proceedings.

Prof. Papadopoulos is a Senior Member of the AIAA and a member of the ASME, the Technical Chamber of Greece (TEE), and the Sigma Xi.

Bin Mu received the B. Eng. and M.Eng. degrees from McGill University, Montreal, QC, Canada, in 1994 and 1996, respectively, all in mechanical engineering.

He was a Staff Engineer at CAE Electronics, Montreal, QC, Canada, from 1996 to 1997. Since 1997, he has been a Consulting Engineer with Adept Technology, Cincinnati, OH, and is now a Systems Engineer with the same company at Livermore, CA. His professional interests are in the area of robotics, servo/motion control, precision assembly technology and microelectromechanical systems.

Réal Frenette received the Bachelor's degree in engineering physics from Université Laval, Laval, QC, CA, in 1982, and the Master's degree in electrical engineering from the University of British Columbia,Vancouver, BC, Canada, in 1985.

From 1985 to 1991, he was a Research Engineer in the Electrical Engineering Department, University of British Columbia. From 1991 to 1993, he was a Research Engineer at the Research and Development Center for Kayaba in Sagamihara, Japan, and from 1994 to 1997, he was a Research Engineer at Centre di Recherche Informatique de Montreal (CRIM), Montreal, QC, Canada in the field of robotics applied to forestry equipment. Since 1998, he has been a Project Engineer for Autolog, Laval. His professional interests are in the area of applied control and forestry automation systems.